

# A Mechanically Intelligent and Passive Gripper for Aerial Perching and Grasping

HaoTse Hsiao<sup>1</sup>, Jiefeng Sun<sup>1</sup>, Haijie Zhang<sup>1</sup>, and Jianguo Zhao<sup>1</sup>

**Abstract**—Perching onto an object (e.g., tree branches) has recently been leveraged for addressing the limited flight time for flying robots. Successful perching needs a mechanical mechanism to damp out the impact and robustly grasp the object. Generally, such a mechanism requires actuation for grasping. In this paper, we present a fully passive mechanism without using any actuator: a mechanically intelligent and passive (MIP) gripper that can be used for either aerial perching or grasping. Initially open, the gripper can be closed by the impact force during perching. After closure, if a sufficient weight (e.g., the robot’s weight) is applied, the gripper can switch to a holding state and maintain that state to hold the weight. Once the weight is removed, the gripper can automatically open. We establish static models for the gripper to predict the required forces for successful state transitions. Based on the models, we develop design guidelines for the gripper so that it can be used for different flying robots with different weights. Experiments are conducted to validate the models. Attaching the gripper onto a quadcopter, we demonstrated aerial perching onto rods and aerial grasping rod-like objects. Because the MIP gripper is lightweight (can reach a mass ratio of 0.75% between the gripper and the grapsed object for static grasping), we expect it would be well suited for aerial perching or grasping due to the limited payload capability for flying robots.

**Index Terms**—Aerial Perching, Grasping, Gripper, Mechanical Intelligence

## I. INTRODUCTION

Biological flyers (e.g., birds) can perch onto tree branches or power lines to rest, saving energy for flights [1], [2]. Inspired by biological flyers, perching has recently been leveraged for aerial robots, especially quadcopters, to address their limited flight time. After perching, they can still monitor a given area but without consuming energy required for staying airborne, enabling long-duration monitoring or surveillance. Successful perching necessitates two types of intelligence [3]: 1) computational intelligence, i.e., algorithms that can estimate, plan, and control the robot’s motion [4], [5]; 2) physical intelligence [6], i.e., perching mechanisms that can damp out the perching impact and grasp the intended perching object [7]. While computational intelligence is critical for successful perching, properly designed mechanisms (e.g., grippers) with physical intelligence can enable perching without precise motion control, alleviating the burden for computational intelligence [8]. The embodiment of intelligence into a robot body has also been investigated for many other robotic systems, especially soft robots [9].

This work is partially supported by National Science Foundation under grants IIS-1815476.

<sup>1</sup>HaoTse Hsiao, Jiefeng Sun, Haijie Zhang, and Jianguo Zhao are all with the Department of Mechanical Engineering at Colorado State University, Fort Collins, CO, 80523, USA

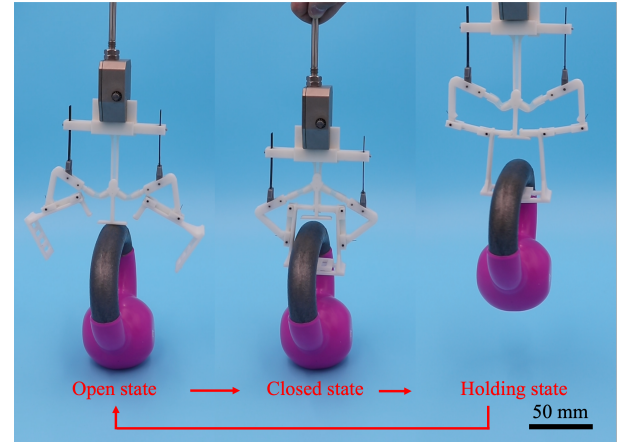


Fig. 1: The MIP gripper passively grasps and lifts a 2.27 kg kettlebell (left: open state; middle: closed state; right: holding state). See the supporting video for the grasping process.

Researchers have recently investigated the physical intelligence for perching by developing various perching mechanisms (recent comprehensive reviews in [1], [10]). Since our gripper is intended for perching onto rod-like objects, we briefly review some representative designs for rod perching. Most designs for rod perching embody a gripper structure, and many of them require actuators (e.g., DC motor, Servos, pneumatic pump) to either open or close the gripper [11]–[16]. Some designs are purely passive, relying on the drone’s weight to close or open the gripper [17]–[19]. Besides grippers, a grapple with microspines has been investigated for perching onto different objects [20]. However, existing grippers used for both perching and grasping usually have a large weight compared with the robot’s weight (mass ratio > 10%) due to the actuators. It remains largely unknown if it is possible to develop a fully passive gripper that can be used for both perching and grasping. Such a gripper can be lightweight without actuators and control circuits, allowing the robot to carry other useful payloads.

In this paper, we present the design, analysis, and experiments for a mechanically intelligent and passive (MIP) gripper (Fig. 1) for either aerial perching or grasping. With a mass of 28 g, the MIP gripper can passively grasp and hold a weight of 3.7 kg, enabling a mass ratio between the gripper and the object to be 0.75% for static grasping (see our supporting video). Consider grasping as an example (the same principle applies to perching). The gripper initially stays at an open state (left of Fig. 1). When it contacts a kettlebell, it can close due

TABLE I: Comparison of existing grippers for rod perching.

Existing grippers	Actuators	gripper weight	total weight	mass ratio	Task
Modular landing gears [3]	Servo	318 g	1438 g	22%	Perching
NTU gripper [11]	Servo	500 g	1800 g	28%	Perching
Avian-Inspired [17]	None	478 g	533 g	90%	Perching
Sarrus-Based [18]	None	20 g	204 g	10%	Perching
Bird Inspired [14]	Servo	89.2 g	567.2 g	16%	Perching
Microspine Grapple [20]	None	32 g	1766 g	2%	Perching
Passive Perching [21]	None	170 g	850 g	20%	Perching
Soft drone [22]	DC motor	200 g	1900 g	11%	Grasping
AGRASP [12]	Servo	372 g	2300 g	16%	Perching or grasping
Passive magnetic grasping [13]	Servo	292 g	770 g	38%	Grasping
Passive closing [15]	Servo	551 g	833 g	66%	Perching or grasping
Bistable [8]	DC motor	13 g	40 g	33%	Perching
<b>MIP Gripper (This work)</b>	<b>None</b>	<b>28 g</b>	<b>593 g</b>	<b>5%</b>	<b>Perching or grasping</b>

to the contact force from the kettlebell's handle. In this closed state, the gripper encloses the kettlebell's handle (middle of Fig. 1). If the gripper is lifted up, it can hold the kettlebell with the holding state (right of Fig. 1). Finally, if the gripper is lowered down to let the kettlebell touch the ground, it can automatically open to release the kettlebell to return to the original open state.

We compare our MIP gripper with closely related grippers in Table I. The table suggests the MIP gripper distinguishes itself in two aspects. First, it has a small mass ratio between the gripper and the flying robot 5%. Second, the MIP gripper can be used for either perching when the gripper is installed at the top of a drone or grasping when installed at the bottom (last column in Table I), whereas most of the other designs only demonstrated a single task. Further, we can easily adjust a single element (details in section III-C) in the gripper to allow for grasping or perching for flying robots with different weights and payload capabilities.

The MIP gripper is based on our recent bistable gripper [8], [23], which allows a quadcopter to passively perch onto a rod by directly using the impact force during perching. However, our previous gripper suffers from several problems. First, it is not fully passive, requiring a DC motor to open the gripper by actuating a lever mechanism, resulting in a complicated design with a large weight (mass ratio between the gripper and the quadcopter is 33%). Second, even though we don't need to precisely control the perching process, we need to precisely control the releasing process. Once the gripper opens, we need to instantly turn on the drone's motors to generate upward thrust forces to prevent the drone from falling to the ground. Third, our previous gripper can only hold a small weight because a weight larger than the maximum switching force will open the gripper.

The MIP gripper can address the shortcomings of our previous bistable gripper: 1) it is fully passive by directly leveraging the impact force to close the gripper, the drone's weight to maintain the closed state, and a special design of extended fingers to open the gripper; 2) it does not need precise control for both perching and releasing. During releasing, we turn on the drone's motor first, after which the gripper will automatically open, simplifying the control process for releasing; 3) it can hold a large weight (132 times its own weight), making the gripper suitable for perching with heavy drones as well as grasping heavy objects.

The advantages of MIP gripper compared with our previous bistable gripper come from a significant redesign and analysis. First, we realize the fully passive design by using a pair of extended fingers with a latch and passive folding capability. The latch will enable the holding state to make the gripper remain closed and hold the weight when an external force is applied, whereas the passive folding capability allows the extended fingers to fold back to their original state when the external force is removed (detailed working principle in section II). Because of the extended fingers, theoretical models for analyzing the forces are also different and more challenging. Second, we can adjust the forces required for perching or grasping by changing the length of two vertical beams in the gripper. This design enables the MIP gripper to be easily adjusted to perch for flying robots with different weights or grasp objects with different weights.

The main contribution of this paper is twofold. First, we present a fully passive and adjustable gripper that can be used for different flying robots for aerial perching or grasping tasks. Such a mechanically intelligent gripper can alleviate the requirement for computational intelligence. Second, we establish theoretical models to predict the required forces for passively opening and closing the gripper. Based on the models, we establish a design guideline for how to adjust the length of the vertical beam for different flying robots to allow successful perching or grasping.

The rest of this paper is organized as follows. In Sec. II, we introduce the working principle and design of the MIP gripper. In Sec. III, we establish analytical models to predict the forces to open and close the MIP gripper. In Sec. IV, we conduct experiments to verify the models; we also perform the grasping and perching experiments to demonstrate the gripper's capabilities. In Sec. V, we discuss the limitations of the MIP gripper and how to address the limitations.

## II. DESIGN OF THE MIP GRIPPER

The MIP gripper can both open and close passively using a compliant mechanism [24]. This is accomplished by combining a bistable mechanism with a pair of extended fingers. In this section, we introduce the bistable mechanism in the gripper, the design of the gripper, and its working principle.

## A. A Bistable Mechanism for the MIP Gripper

The MIP gripper is based on a bistable mechanism as shown in Fig. 2. The bistable mechanism is made from a pair of vertical beams rigidly connected to a base. A pair of fingers is connected to the beams through revolute joints. The fingers are connected to a switch part in the middle via two compliant joints. With this design, the mechanism will have two stable states: top and bottom stable states. With the mechanism initially at the bottom stable state (left of Fig. 2), if an upward force  $F_1$  is applied to the switch part, the beams will bend outward, and the mechanism will switch to the top stable state (right of Fig. 2). In this top state, if a downward force  $F_2$  is applied to the switch part, the mechanism can switch back to the bottom stable state. A detailed investigation of the bistable mechanism can be found in [8].

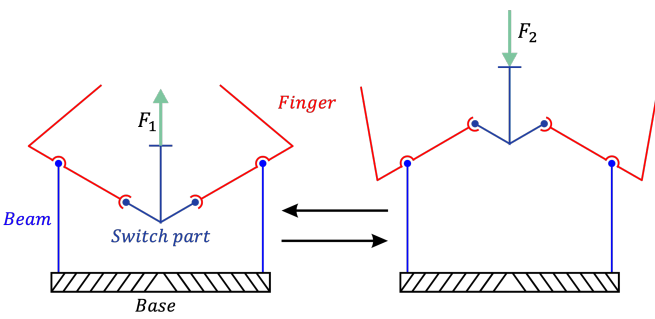


Fig. 2: A bistable mechanism with two stable states: top (right figure) and bottom (left figure). If the mechanism is initially at the bottom state, it can switch to the top stable state when  $F_1$  is applied to the switch part. It can switch from top back to bottom state when  $F_2$  is applied.

## *B. Design of the MIP Gripper*

The MIP gripper is developed based on the bistable mechanism. It consists of a rigid base, two adjustable vertical beams attached to the base, two fingers connected to the beams through a revolute joint ( $J_3$  in Fig. 3), two intermediate links connected to the fingers through another revolute joint ( $J_1$  in Fig. 3), two extended fingers connected to the intermediate links through revolute joint  $J_2$ , and a switch part connected to the fingers through two elastic tubes as compliant joints (CJs). If we don't have the two intermediate links and the two extended fingers, the remaining parts become the bistable mechanism discussed in section II-A.

Because the motion of extended fingers is not constrained, we place a torsion spring at  $J_1$  and  $J_2$ , respectively. Both springs are pre-tensioned so that the extended fingers can be folded to be in the open configuration when the bistable mechanism is at the top stable state.

Each of the two extended fingers includes an upper extended finger (UEF) and a lower extended finger (LEF) (Fig. 3). The right UEF has some grids, whereas the left UEF has a protrusion that can insert into the grids for latching if an upward force is applied. But when no upward force is applied, the two UEFs are designed to be separate from each other (the left UEF is lower than the right UEF). The two LEFs are under the impact pad of the switch part so that they can contact the impact pad to remain in the holding state when an upward force is applied to the UEFs.

The length of the two vertical beams can be adjusted using two screws on the rigid base. This allows the gripper to be used for different flying robots (details on how to determine the beam's length will be discussed in Sec. III-C). We also designed a linear guide to ensure the switch part can only move vertically without side movements. This guide is realized by using two small screws attached to the switch part, but the screws can slide along a groove in the guide.

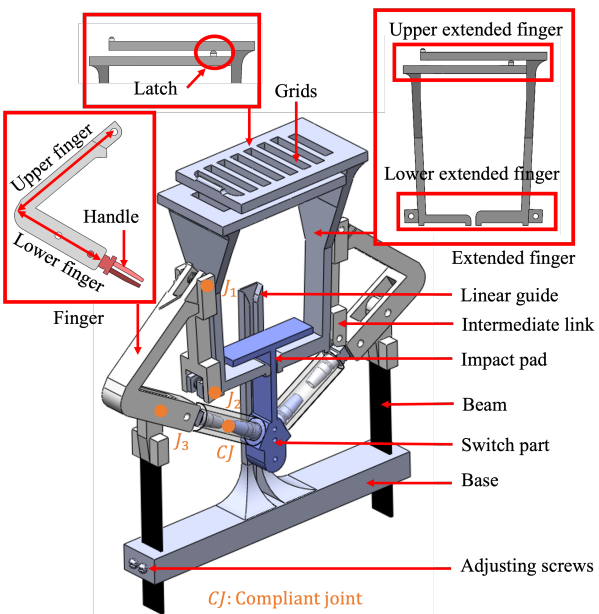


Fig. 3: Structure and key components of the MIP gripper.

### C. Working Principle of the MIP Gripper

We explain the working principle with a simplified sketch (Fig. 4) using perching as an example (the same principle applies to grasping). Consider the case when the gripper is placed on the top of a drone to allow it to perch onto a rod. Also assume the gripper is initially open (state  $S_o$ , the top of Fig. 4). Starting from  $S_o$ , the gripper can switch to the closed state  $S_c$  (bottom left of Fig. 4), and then to an holding state  $S_h$  (bottom right of Fig. 4), and finally return to the original open state  $S_o$ . In the following, we explain the transitions of the three states.

**Process  $P_{oc}$  (from  $S_o$  to  $S_c$ ):** As the drone flies upward, the gripper will contact the rod, resulting in a downward force  $F_d$  applying on the switch part (top of Fig. 4). This  $F_d$  will switch the bistable mechanism to the bottom stable state  $S_c$ , closing the gripper to encircle the rod inside the two extended fingers.

**Process  $P_{ch}$  (from  $S_c$  to  $S_h$ ):** With the rod inside the two extended fingers, we can turn off the motors of the drone. In this case, the drone's weight must be balanced by an upward force ( $F_u$ ) applied to the extended figures (left of Fig. 4). This

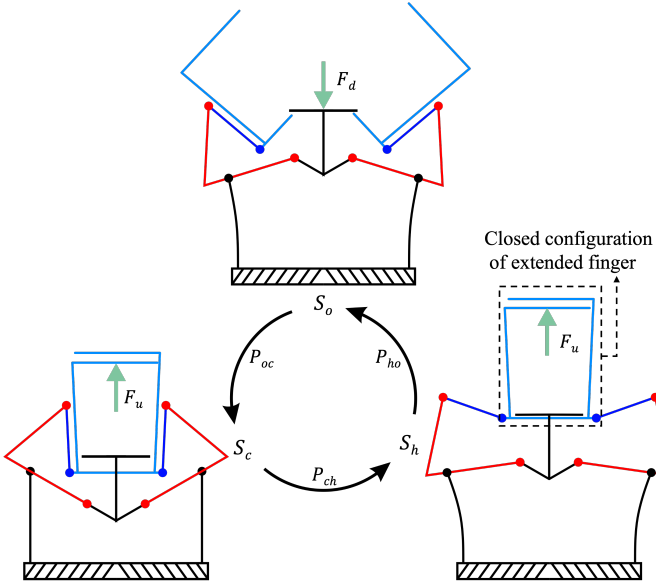


Fig. 4: Illustration of the MIP gripper's working principle. Top sketch: open state  $S_o$ ; bottom left sketch: closed state  $S_c$ ; bottom right sketch: holding state  $S_h$ .

force  $F_u$  will first latch the two UEFs and push the extended fingers upward to switch the bistable mechanism to the top stable state. During this process, the extended fingers remain closed because the two UEFs are latched together due to  $F_u$ . Eventually, the gripper will be in an holding state  $S_h$  (right of Fig. 4). In this case, the drone can hang on the rod without any additional energy input.

**Process  $P_{ho}$  (from  $S_h$  to  $S_o$ ):** When we turn on motors of the drone to generate thrust, the gripper can switch from  $S_h$  to  $S_o$ . During this process, the upward force ( $F_u$ ) applied to the extended fingers disappears since the thrust can balance the drone's weight. The two UEFs can thus de-latch from each other because they are designed to be separate from each other when no upward force is applied. Because of the torsional springs at joints  $J_1$  and  $J_2$ , the extended fingers will fold back to their original configuration, opening the gripper to return to state  $S_o$ .

To ensure the successful switching between the three states  $S_o$ ,  $S_c$ , and  $S_h$ , we need to have the following conditions. (1) Process  $P_{oc}$  (from  $S_o$  to  $S_c$ ). The impact force  $F_d$  should be large enough to switch the state for the bistable mechanism. This means the drone should have a enough thrust force to generate the required impact force. (2) Process  $P_{ch}$  (from  $S_c$  to  $S_h$ ).  $F_u$  should be large enough to switch the state of the bistable mechanism, and it can be quite large as long as the gripper does not break. (3) Process  $P_{ho}$  (from  $S_h$  to  $S_o$ ). To ensure this process, the bistable mechanism should maintain its bistability, i.e., it should not go back to its initial bottom state. All of these conditions will be used to develop a design guideline in section III-C for obtaining the proper length for the vertical beams to ensure successful perching for different drones and grasping different weights.

### III. MODELING OF THE MIP GRIPPER

To ensure successful switching of states, we need to predict how  $F_u$  on extended fingers will change with respect to the vertical displacement of the extended fingers (denoted as  $x$ ), how  $F_d$  on the switch part will change with respect to the vertical displacement of the switch part (denoted as  $d$ ), i.e., force profile  $F_u(x)$  and  $F_d(d)$ . For perching,  $F_d(d)$  will determine the minimum required impact force to close the gripper, and  $F_u(x)$  will determine the minimum weight of the drone to open the gripper. In this section, we discuss how to solve  $F_u(x)$  and  $F_d(d)$  separately.

#### A. Profile for Upward Force on Extended Fingers: $F_u(x)$

Some fixed geometric parameters are shown in Fig. 5 for the MIP gripper in  $S_c$ . They will be explained later in this section. A diagram for the gripper during  $P_{ch}$  is shown in Fig. 6. The displacement of the extended finger in the vertical direction changes with respect to  $F_u$  during  $P_{ch}$ . Note that  $x$  is different from the displacement of the switch part  $d$ .  $F_u$  with respect to  $x$  during  $P_{ch}$  can be obtained using the Theorem of Least Work by considering the total strain energies ( $E_{tot}$ ):

$$F_u(x) = \frac{\partial E_{tot}}{\partial x} = \frac{\partial E_{tot}}{\partial d} \frac{\partial d}{\partial x} \quad (1)$$

where  $E_{tot} = E_b + E_t + E_{s1} + E_{s2}$ , with  $E_b$  as strain energies in the two beams,  $E_t$  as strain energies in the two CJs,  $E_{s1}$  and  $E_{s2}$  as strain energies in torsion springs placed at  $J_1$  and  $J_2$ , respectively. Since the four strain energies can be easily represented in terms of  $d$  instead of  $x$ , we use  $d$  as an intermediate variable, and first take the derivative with respect to  $d$ :  $F_u(d) = \partial E_{tot}/\partial d$ , and then obtain  $F_u(x)$  by multiplying  $F_u(d)$  with  $\partial d/\partial x$  [Eq. (1)]. In the following, we derive the individual energies for  $E_b$ ,  $E_t$ ,  $E_{s1}$ , and  $E_{s2}$ . Then, we will solve  $F_u(d)$ , and  $\partial d/\partial x$  to eventually obtain  $F_u(x)$ .

First, the total strain energy from two beams  $E_b$  can be approximated as two linear springs because of the small bending [8]:

$$E_b = k_d d_b^2 \quad (2)$$

where  $k_d$  is the spring constant.  $d_b$  is the horizontal displacement of the bending beams that can be derived from a geometrical relationship:  $H^2 + L_0^2 = (H - d)^2 + (L_0 + d_b)^2$ , where  $H$  and  $L_0$  are constants (Fig. 6) at the initial configuration  $S_c$  that can be obtained by:  $H = (l_f + \gamma l_t) \sin \theta_0$  and  $L_0 = (l_f + \gamma l_t) \cos \theta_0$ , where  $\theta_0$  is the angle between the horizontal line and the lower finger at  $S_c$ .  $l_f$  is length from  $J_3$  to the end of lower finger's handle.  $l_t$  is distance between the handles of the lower finger and switch part, and  $\gamma$  is a ratio to locate bending point for the tube if we use a pseudo-rigid-body model to approximate the tube's bending [8]. Then, we can solve  $d_b$  as a function of  $d$ :  $d_b = \sqrt{L_0^2 + 2Hd - d^2} - L_0$ .

Second, the total strain energy of two compliant joints (CJs)  $E_t$  is

$$E_t = k_\theta (\theta_1 - \theta_0)^2 \quad (3)$$

where  $k_\theta$  is the spring constant of the CJ, which can be experimentally obtained (details in Sec. IV).  $\theta_1 =$

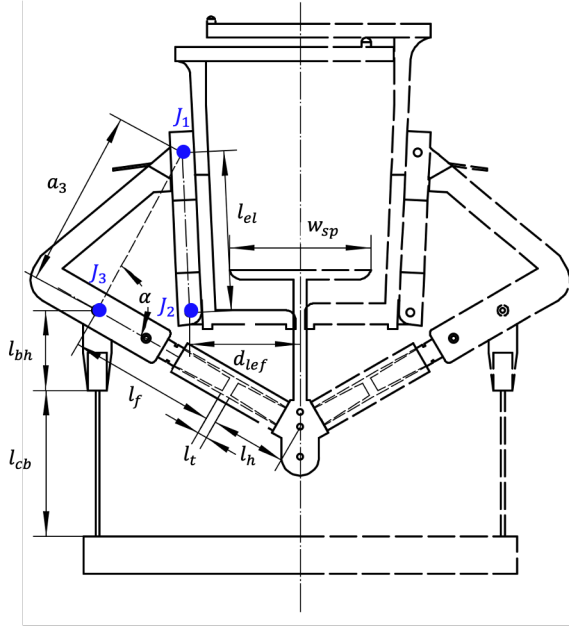


Fig. 5: Front view of the gripper. The geometric parameters are labeled in left half since the gripper is symmetrical with respect to its center.

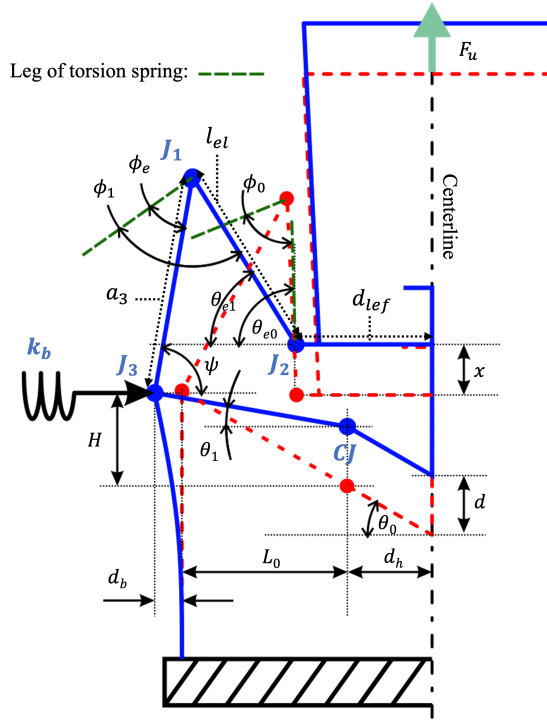


Fig. 6: The schematic showing the  $P_{ch}$ . The red dash lines represent the initial closed state ( $S_c$ ), whereas the solid blue lines represent the gripper when the switch part moves up by a distance of  $d$ . Since the gripper is symmetrical, only half of the gripper is shown.

$\arctan[(H - d)/(L_0 + d_b)]$  is the angle between the horizontal line and the lower finger at the CJ during the process  $P_{ch}$  (blue line).

Third, the torsion springs at  $J_1$  have a pre-rotating angle  $\phi_0$  when the gripper is in the closed state  $S_c$ , and it will increase to  $\phi_1$  when the extended fingers move up for a displacement of  $x$  (Fig. 6). The total strain energy  $E_{s1}$  of two springs at  $J_{1s}$  can be written as:

$$E_{s1} = k_{s1}\phi_1^2 \quad (4)$$

where  $k_{s1}$  is spring constant of the torsional spring,  $\phi_1 = \pi - \theta_{e1} - \psi + \phi_e$  where  $\phi_e$  is an angle between the leg of torsion spring and a virtual link connecting  $J_1$  and  $J_3$ ,  $\theta_{e1} = \arccos[(d_b + L_0 + d_h - a_3 \cos \psi - d_{lef})/l_{el}]$  is the angle between horizontal line and intermediate link,  $d_h$  is distance from the CJ to the centerline,  $l_{el}$  and  $d_{lef}$  are respectively the length of the intermediate link and the lower extended finger,  $a_3$  is the length of the virtual link between  $J_1$  and  $J_3$ ,  $\psi = \alpha - \theta_1$  is the angle between the virtual link and horizontal line, and  $\alpha$  is the angle between the the virtual link and the lower finger.

Fourth, the torsion springs at  $J_2$  also have a pre-rotating angle  $\theta_{e0}$  which is between the horizontal line and intermediate link at  $S_c$ . The total strain energy of these two springs  $E_{s2}$  can be written as:

$$E_{s2} = k_{s2}(\pi - \theta_{e1})^2 \quad (5)$$

where  $k_{s2}$  is the spring constant of the torsional spring. The initial value of  $\theta_{e1}$  is  $\theta_{e0}$ .

Based on the individual energies, we can obtain  $E_{tot}$  to solve for  $F_u(d) = \partial E_{tot}/\partial d$  in Eq. (1) as:

$$F_u(d) = \frac{-2}{a_3 \cos \psi + A \cot \theta_{e1}} \left[ k_b d_b (H - d) + \frac{A}{l_{el} \sin \theta_{e1}} \times (k_{s1}\phi_1 + k_{s2}(\pi - \theta_{e1})) - k_\theta(\theta_1 - \theta_0) - k_{s1}\phi_1 \right] \quad (6)$$

where  $A = H - d + a_3 \sin \psi$ .

Finally, the relationship between  $d$  and  $x$  is required for solving  $\partial d/\partial x$  in Eq. (1). Since we assume  $J_3$  can only displace horizontally,  $x$  can be solved from the vertical distance between  $J_3$  and  $J_2$ :  $x = a_3 \sin \psi - l_{el} \sin \theta_{e1} + d_{(J_3, J_2)}$ , where  $d_{(J_3, J_2)}$  is initial vertical distance between  $J_3$  and  $J_2$ . Therefore, we can obtain  $\partial x/\partial d$  as

$$\frac{\partial x}{\partial d} = (L_0 + d_b)/[a_3 \cos \psi + \cot \theta_{e1}(H - d + a_3 \sin \psi)]$$

With  $F_u(d)$  and  $\partial x/\partial d$ , we can plug them into Eq. (1) to solve for  $F_u(x)$ .

### B. Profile for Downward Force on Switch Part: $F_d(d)$

During the process of  $P_{oc}$ , the downward force  $F_d$  applied to the impact pad can displace the pad to close the gripper. Note that intermediate links and extended fingers will not participate in the process because they are folded. In this case, we can simplify the sketch as shown in Fig. 7.  $F_d$  with respect to  $d$  can still be solved from the total energy  $E_{tot}$ :

$$F_d(d) = \frac{\partial E_{tot}}{\partial d} \quad (7)$$

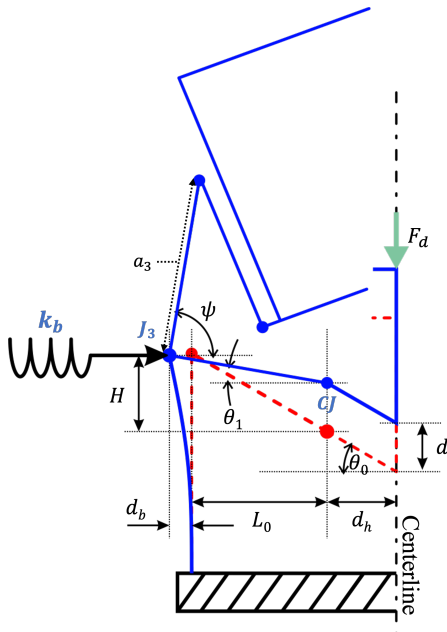


Fig. 7: Schematic showing  $P_{oc}$ .  $F_d$  will change with respect to  $d$ . Blue lines is corresponding to the

where  $E_{tot} = E_b + E_t$  with  $E_b$  the total strain energy from the beams and  $E_t$  the total strain energy from the tubes (derived in Sec. III-A).

Solving Eq. (7), we can obtain  $F_d$  with respect to  $d$  during  $P_{oc}$  as:

$$F_d(d) = \frac{2}{L_0 + d_b} [k_d d_b (H - d) - k_\theta (\theta_1 - \theta_0)] \quad (8)$$

Unlike Eq. (6), Eq. (8) is simpler because we don't need to consider the extended fingers and the intermediate links since they are folded.

### C. Design Guidelines of the MIP Gripper

Based on the profiles  $F_u(x)$  and  $F_d(d)$ , we can develop design guidelines for the MIP gripper: how should we design the gripper so that it can successfully allow a drone to perch onto a rod or grasp a given payload. We aim to develop a framework for designing an adjustable MIP gripper that can be used for different drones. Since there are many geometric parameters in the gripper, we simplify the design problem by choosing a parameter that can be easily adjusted while fixing all the other parameters. This parameter is the bending stiffness of the vertical beam  $k_b$  since it can be easily adjusted by changing its length using screws at the base (Fig. 3).

We use perching to establish the design guidelines and discuss how to apply the guidelines to grasping at the end of this section. Assume a drone has a maximum thrust force of  $F_t$  and a weight of  $F_w$ . To enable successful perching using the MIP gripper, we need to guarantee three conditions discussed at the end of section II-C to allow successful state switching.

**Process  $P_{ho}$  (from  $S_h$  to  $S_o$ ):** To ensure this process, the bistable mechanism should maintain its bistability so that when  $F_u$  is removed, the bistable mechanism can stay in the top stable state to allow the gripper to automatically open.

According to the bistability analysis in [8],  $k_b$  should be large enough. This means for a given  $k_b$ , the maximum value of profile  $F_d(d)$  should be positive. We denote this maximum value as  $F_{d,max}(k_b)$  since it changes with respect to  $k_b$ . Therefore, to ensure a successful transition from  $S_h$  to  $S_o$ , we have:

$$F_{d,max}(k_b) > 0 \quad (9)$$

**Process  $P_{oc}$  (from  $S_o$  to  $S_c$ ):** The impact force should be large enough to switch the state from  $S_o$  to  $S_c$ . This means  $k_b$  should be small enough so that the drone's maximum thrust force  $F_t$  can result in a sufficient impact force to switch the state. Since it is complicated to determine impact force dynamics, we simplify the problem by considering the maximum upward quasi-static force that can be generated by the drone,  $F_t - F_w$ , which represents the lower bound of the maximum impact force. Therefore, to ensure a successful transition from  $S_o$  to  $S_c$ , we have:

$$F_{d,max}(k_b) < F_t - F_w \quad (10)$$

**Process  $P_{ch}$  (from  $S_c$  to  $S_h$ ):** In this case,  $k_b$  should also be small enough so that the drone's weight  $F_w$  can successfully switch the state from  $S_c$  to  $S_h$ . The maximum value of profile  $F_u(x)$  (denote as  $F_{u,max}(k_b)$ ) should be less than  $F_w$ . Therefore, we can have another inequality:

$$F_{u,max}(k_b) < F_w \quad (11)$$

With the three inequalities (9) to (11), we can numerically solve for a range for  $k_b$  given  $F_t$ ,  $F_w$ , and other geometric parameters for the gripper. For instance, for the drone (593 g) that will be used in our experiments in section IV, it has  $F_w = 5.28$  N and a maximum thrust force of  $F_t = 8.89$  N. If we use this drone for perching, we can use Matlab to numerically find  $420.7 < k_b < 2048$  Nm<sup>-1</sup>.

The same design framework applies to aerial grasping when the gripper is placed at the bottom of a drone. To ensure successful grasping, Eq. (9) is the same since we still need to ensure the bistability. For Eq. (10), we need to consider two cases. If the drone needs to land on the ground to grasp, then  $F_t - F_w$  should be changed to  $F_w$  since the drone will rely on its weight to switch the state from  $S_o$  to  $S_c$ . If the drone needs to grasp without landing on the ground, then  $F_t - F_w$  should be changed to  $F_w - F_{minThrust}$ , where  $F_{minThrust}$  is the additional thrust applied to keep the drone airborne. For Eq. (11), we need to change  $F_w$  to the weight of the object that will be grasped. For instance, if we want a drone to grasp an object of 260 g by landing on the ground, then we can solve the three inequalities to get  $420.7 < k_b < 661.2$  Nm<sup>-1</sup>. Therefore, if we use the same gripper to be placed on a drone with a mass of 593 g for either perching or grasping an object of 260 g, then the range of  $k_b$  should be  $420.7 < k_b < 661.2$  Nm<sup>-1</sup>.

With the range of  $k_b$ , we can further determine the range of length of the vertical beams ( $l_{cb}$  in Fig. 5), which can be adjusted using two screws in our design. Although we can obtain the analytical solution for  $k_b$  with respect to  $l_{cb}$ , we experimentally obtain such a relationship for a better accuracy. Fig. 8 shows how  $k_b$  will change with respect to  $l_{cb}$  from

27 to 35 mm. Since  $l_{cb}$  is linear with respect to  $k_b$ , we can get the trend line function  $l_{cb} = -0.025k_b + 47.5$  to get the corresponding  $l_{cb}$  for different  $k_b$ . Therefore, if we want to use the same gripper to allow for a drone weighing 593 g to perch or grasp an object weighing 260 g, the length of the vertical beam should be in a range  $30.97 < l_{cb} < 36.98$  mm.

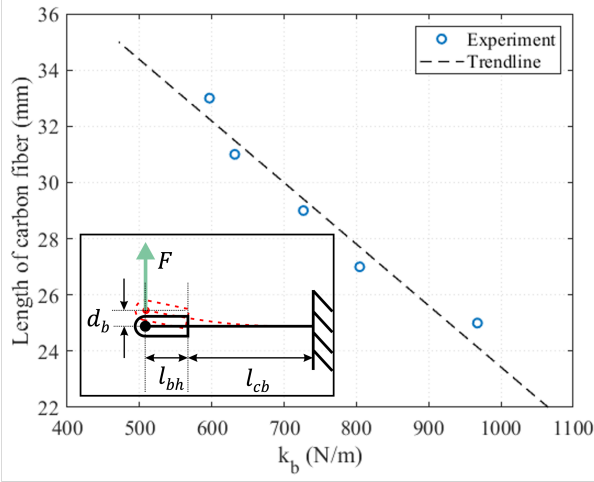


Fig. 8: Experimental results for the relationship between  $k_b$  and  $l_{cb}$  from experiment:  $l_{cb} = -0.025k_b + 47.5$ . The experimental setup is shown inside the plot.

#### IV. EXPERIMENTS AND RESULTS

In this section, we elaborate on the fabrication of the MIP gripper, verify the mathematical model developed in Sec. III with experimental results, and conduct grasping and perching experiments to demonstrate the capability of the gripper.

Note that all experiments about the force measurement are conducted using a motorized test stand (ESM303, Mark-10), which can measure the force and displacement at the same time. For example, Fig. 9 shows the experimental setup for measuring the upward force with respect to displacement during  $P_{ch}$ .

##### A. Gripper Fabrication

The main design parameters of the gripper are listed in Table II. Most rigid parts (e.g., the fingers, extended fingers, intermediate links, base, etc.) are 3D printed (Ender-3 pro) with PLA materials. To generate reliable forces during bending and allow for length adjustment, the two vertical beams are carbon fiber plates (Width×Thickness: 7.9 × 0.8 mm, CF312032048, Goodwinds Composites LLC) as opposed to previous beams made from PLA [8]. To connect the plates to the fingers through joint  $J_3$ , two 3D-printed beam heads are used. For the two CJs, the tube (ULTRA-C-062-3, SainTech) has inner and outer diameters of 1.6 mm and 6.35 mm, respectively. The width of the impact pad  $w_{sp}$  should be close to two times of  $d_{lef}$  for blocking the two lower extended fingers during  $P_{ch}$  (Fig. 5). The spring constants used in our gripper are listed in Table II and discussed below:

- Linear spring constant  $k_b$  for beams: Since the beam head ( $l_{bh}$ ) is part of beams during bending,  $k_b$  cannot

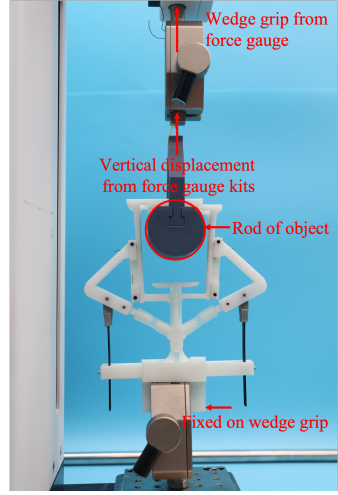


Fig. 9: Experimental setup for measuring the upward force during  $P_{ch}$ . The gripper is fixed on a wedge grip and a cylindrical rod connected the force gauge will drag the gripper to switch the state.

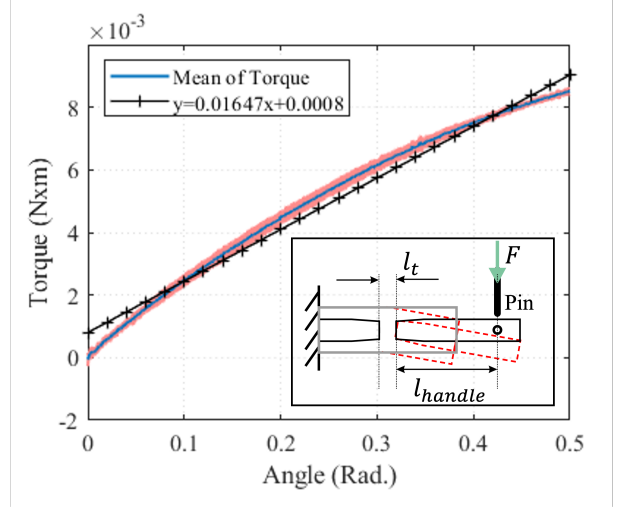


Fig. 10: Experimental results for the spring constants of the tube. The plot shows  $k_\theta$  can be approximated as  $0.01647$  N/m. The red shaded area shows the standard deviation from 3 experiments. The experimental setup is shown inside the plot.

be calculated from the carbon fiber plates' dimensions directly. Therefore, we experimentally obtain  $k_b$  with the length of  $l_{cb}$  from 25 to 33 mm. The experiment setup is shown at bottom-left diagram of Fig. 8. We apply an upward force  $F$  to bend the beam. By recording and plotting  $F$  with respect to  $d_b$ , we can obtain the value of  $k_b$  for a given length  $l_{cb}$ . We conduct the experiments for different  $l_{cb}$  and plot the results in Fig. 8.

- Torsion spring constant  $k_\theta$  of CJs:  $k_\theta$  is also obtained by experiments. The experimental setup is shown at the bottom-right diagram of Fig. 10. We apply a downward force on the handle through a pin with the point touching on the handle as a free contact. This ensures the moment arm is always constant. We can obtain and plot the

bending angle and the corresponding torque as shown in Fig. 10, from which we can approximate the torsion spring constant for CJs as  $k_\theta = 0.01647$  N/rad.

- Spring constant for torsion springs at  $J_1$  and  $J_2$  are both same  $k_{s1} = k_{s2} = 0.0036$  N/rad (GT1206718-ML, Gardner Spring Inc). Note that we manually modify all the torsion springs to have an initial angle of  $0^\circ$ .

TABLE II: Value for geometric parameters of the gripper.

parameter	symbol	value	unit
initial angle of torsion spring at $J_1$	$\phi_0$	100	degree
angle between spring leg and $a_3$ at $J_1$	$\phi_e$	28	degree
angle between horizontal line and LEF	$\theta_{eo}$	93	degree
vertical distance between $J_3$ and $J_2$	$d_{(J_3, J_2)}$	0.5	mm
length between $J_1$ and $J_2$	$l_{el}$	34.0	mm
distance between $J_2$ and center line	$d_{lef}$	23.4	mm
length between $J_3$ and end of handle	$l_f$	31.5	mm
length between two handles at $CJ$	$l_t$	3.6	mm
length of handle at switch part	$l_h$	14.6	mm
width of impact pad	$w_{sp}$	30	mm
spring constant of beam	$k_b$	650	N/m
effective length of carbon fiber plates	$l_{cb}$	31	mm
spring constant of tube	$k_\theta$	0.01647	N/rad
spring constant for springs at $J_1$	$k_{s1}$	0.0036	N/rad
spring constant for springs at $J_2$	$k_{s2}$	0.0036	N/rad

### B. Profile of Downward Force $F_d(d)$ during $P_{oc}$

To verify  $F_d(d)$  during process  $P_{oc}$ , we conduct three sets of experiments for three different lengths of the carbon fiber plates ( $l_{cb} = 25, 28$  and  $31$  mm) by using the test stand to push the switch part and record both the force and displacement. Fig. 11 shows the comparison between the simulations and the experimental results. Note that the initial displacement  $d$  starts from 0 mm at  $S_o$  and gradually increases until  $F_d$  becomes 0 N, after which the bistable mechanism will automatically switch to the bottom stable state. From the plot, the downward force to close the gripper should be larger than 0.87, 0.65, 0.42 N for  $l_{cb} = 25, 28, 31$  mm respectively in order to close the gripper. The mean error of the force between the simulations and the experiments with  $l_{cb} = 25, 28$  and  $31$  mm are 0.28%, 3.99% and 0.95% respectively. As a result, the theoretical model can accurately predict the force. In this work, we select  $l_{cb}$  to be 31 mm for perching and grasping experiments. Therefore, the downward force should be greater than 0.42 N to close the gripper. The discrepancy between the simulations and experimental results after crossing the maximum of  $F_d$  is mainly because  $k_t$  of the CJs is considered as a constant in the simulation, but it will increase when a longitudinal force is applied to the tube, which is the case when  $d$  becomes larger since the bending of the vertical beam will generate a longitudinal force applied to the tube [8].

### C. Profile of Upward Force $F_u(x)$ during $P_{ch}$

To verify  $F_u(x)$  during process  $P_{ch}$ , we also conduct three sets of experiments for three different lengths of the carbon fiber plates ( $l_{cb} = 25, 28$  and  $31$  mm) by using the test stand (Fig. 9). Fig. 12 shows the comparison between the simulation and experimental results of  $F_u$  with respect to  $x$  when  $l_{cb} = 25, 28$  and  $31$  mm respectively. The figure only shows when

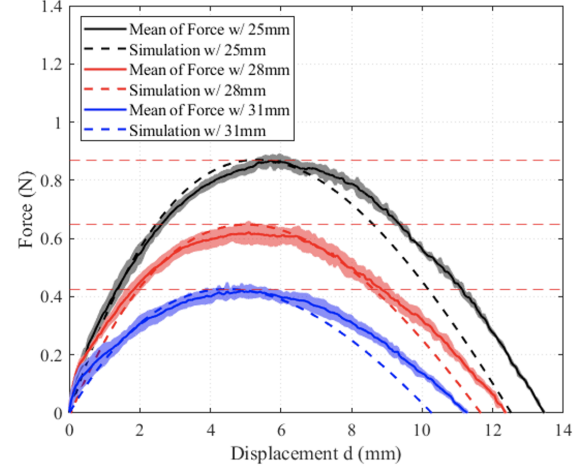


Fig. 11: Downward force  $F_d$  with respect to  $d$  during process  $P_{oc}$ . Different lengths of the carbon fiber plates  $l_{cb}$  are used: 25, 28 and 31 mm. Each shaded area shows the standard deviation from 3 repeated experiments.

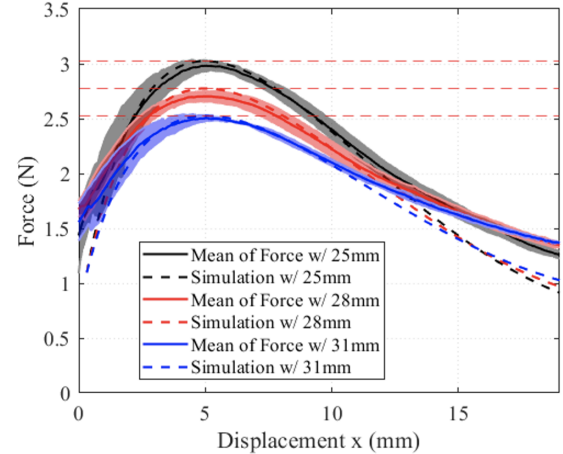


Fig. 12: Upward force  $F_u$  with respect to displacement  $x$  during  $P_{ch}$  with different  $l_{cb}$ : 25, 28 and 31 mm. Each shaded area shows the standard deviation from 3 experiments. The horizontal red dash lines show the maximum of  $F_u$ , which increases when  $l_{cb}$  decreases from 31 to 25 mm.

$x < 20$  mm since when  $x > 20$  mm, the impact pad will prevent the two LEFs from moving (refer to the gripper design in Fig. 3). The mean errors of  $F_u$  between the simulations and experiments are 1.44%, 2.62% and 0.83% respectively for  $l_{cb} = 25, 28$  and  $31$  mm. From the figure, to successful switch the state from  $S_c$  to  $S_h$ , the upward force should be larger than the maximum of  $F_u(x)$ , i.e., 3.03 N, 2.78 N, and 2.53 N for  $l_{cb} = 25, 28$  and  $31$  mm, respectively. This means if the gripper is used for perching, the total weight of the drone with the gripper should be larger than 2.53 N to allow successful passive opening when  $l_{cb} = 31$  mm. Note that after passing the peak of  $F_u$ , there are discrepancies between the simulation and experiments, which should also be mainly due to the nonlinear stiffness of the tube as explained in Sec. IV-B.

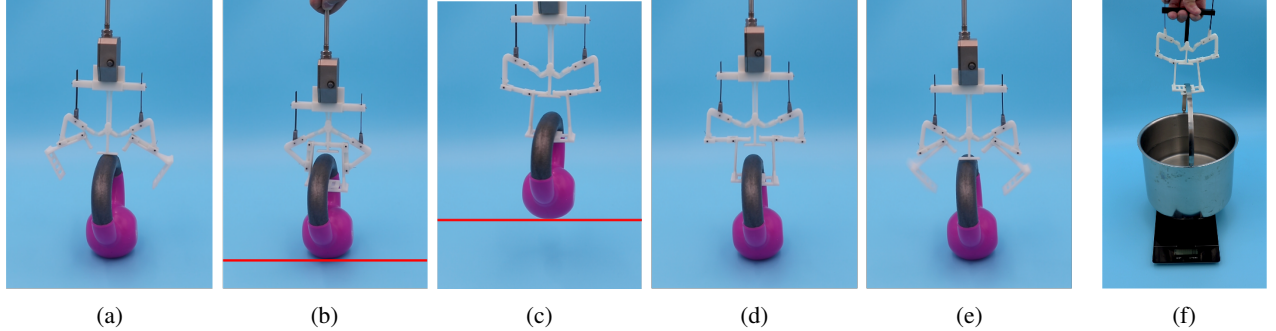


Fig. 13: Grasping experiment. (a) the gripper is open. (b) the gripper contacts the handle of the kettlebell (2.27 kg) to close. (c) the extended fingers keep the closed configuration and lift up the kettlebell. (d) the gripper moves down to put the kettlebell on the ground. (e) when the force is removed from the extended fingers, the gripper opens to release the kettlebell. (f) The gripper can lift up a bucket with water (3.7 kg).

#### D. Static Grasping Experiment

After verifying the model, we demonstrate that the MIP gripper can grasp different heavy objects: a kettlebell (2.27 kg) and a bucket with water (3.7 kg) in Fig. 13 (also see the video supplement). The complete grasping process is demonstrated by grasping the kettlebell. The gripper is installed upside down (Fig. 13a). As the gripper moves down, its impact pad contacts the kettlebell to close the gripper (Fig. 13b). In the holding state, it can lift up the kettlebell (the red lines in Fig. 13b and 13c). Once the gripper moves down until the kettlebell touches the ground, the closed extended fingers open automatically (Fig. 13d and 13e). Fig. 13f shows the gripper can grasp a bucket of 3.7 kg with a thinner handle (the detailed process can be found in the video supplement).

#### E. Perching Experiment

We also demonstrate aerial perching of a quadcopter with the MIP gripper. The gripper is fixed onto the top of a customized quadcopter developed in our lab (565 g without the gripper). The experimental results are illustrated in Fig. 14 (also see the video supplement). The gripper is initially open (Fig. 14a), and it closes upon contacting a fixed rod (Fig. 14b). After the propellers stop rotating, the weight of the quadcopter will be applied to the UEFs to switch the gripper to the holding state, and the quadcopter can rest on the rod (Fig. 14c) without additional energy input. To release from the rod, we simply apply an upward thrust to remove the force applied on the UEFs of the gripper (Fig. 14d).

#### F. Aerial Grasping Experiment

Finally, we demonstrate aerial grasping by attaching the gripper onto the bottom of the quadcopter (Fig. 15, also see the video supplement). Four legs are added to the quadcopter to protect and leave space for the gripper. The target object is 260 g in total and has a handle to facilitate grasping. The quadcopter flies over the object (Fig. 15a). Once the quadcopter moves down to let the gripper's impact pad touch the handle, the impact force will close the gripper (Fig. 15b). Then, the quadcopter flies up, and the gripper switches to a holding state when the object is lifted up (Fig. 15c). After the

quadcopter carries the object in flight, the quadcopter lands, releasing the object (Fig. 15d and 15e). In addition to this object, we also demonstrate that the gripper can be used for grasping a box with a thin handle (225 g) without landing on the ground during the grasping process as shown in Fig. 15e (the detailed process can be found in the video supplement).

## V. DISCUSSIONS

As demonstrated in our experiment, the MIP gripper is purely passive without any actuator, yet it can be used for both aerial grasping and perching. The MIP gripper with a mass of 28 g can lift up a mass of 3.7 kg under a static condition: more than 132 times its own weight. Note that a dynamic load could reduce the ratio, and if it is used to lift a weight larger than 3.7 kg, the gripper might break at some locations: the grids at the UEF, joint  $J_2$ , or the connection between beam head and the beam. However, we believe it can hold even heavier weights if we strengthen those critical parts. This means it can be used for perching or grasping for heavy drones. Because it does not have any actuator, it can be fabricated at a low cost (we estimate the gripper costs around \$4). Because of its mechanical intelligence, it does not need precise position control, alleviating the requirement for computational intelligence. In this case, we believe it can be used for rapidly grasping an object in flight without sophisticated control [22]. We envision that it can be installed on commercially available quadcopters to enable the perching/grasping capability. It can also be added to the end of existing aerial manipulators [25] to facilitate manipulation tasks. Using the gripper for perching or grasping, we need to pay attention to the following aspects. First, the gripper currently only works for rod-like objects, whose size should be smaller than the width of the UEF. If an object is too large, the latch may not be able to insert into the grid of the UEFs, preventing the extended fingers from keeping the closed state when an upper force is applied. To address this issue, we might need to replace the rigid UEFs with some compliant bistable strips [26]. Besides rod-like objects, we believe a similar mechanism should work for perching onto surfaces [10] by attaching a vacuum pad at the end. Second, for grasping tasks, the weight of the object should be large enough to ensure a successful state transition from  $S_c$  to  $S_h$ . In this

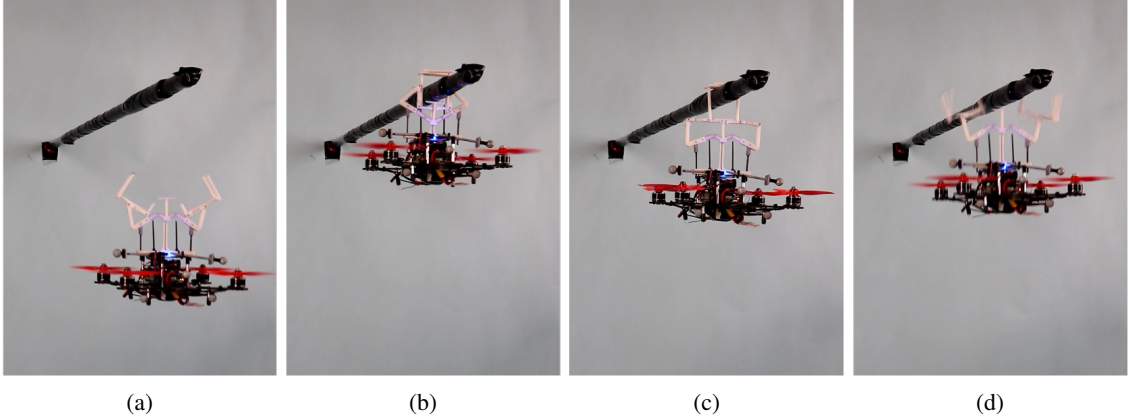


Fig. 14: Perching experiment (a) a quadcopter flies under a rod while the gripper is open. (b) the gripper contacts the rod to close the gripper. (c) the quadcopter’s weight switches the state of the bistable mechanism, but the two extended fingers remain closed to let the quadcopter hang on the rod. (d) an upward thrust opens the extended fingers to release the gripper from the rod, then the quadcopter can fly away.

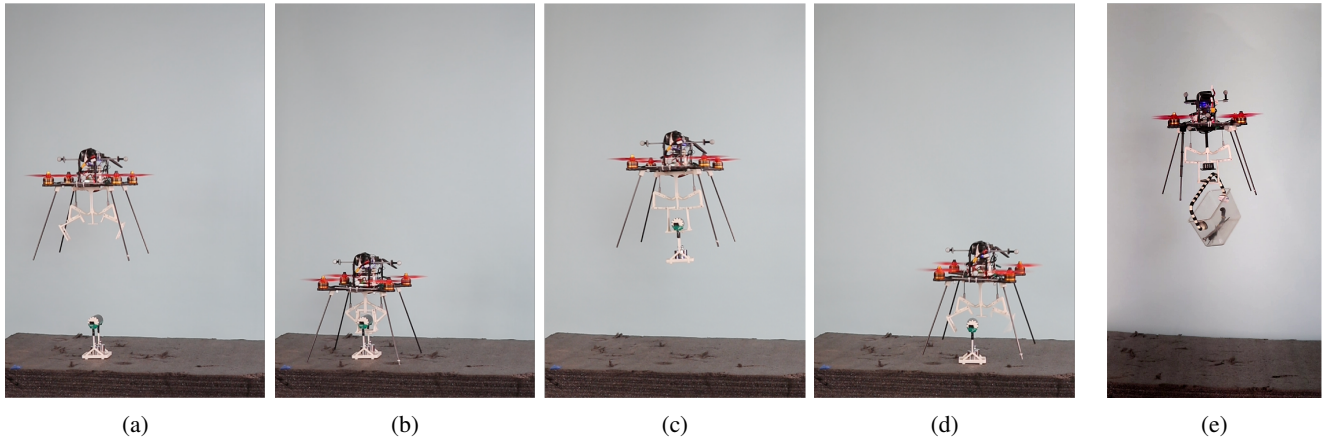


Fig. 15: Aerial grasping experiments. (a) The gripper is open and fixed on the bottom of the quadcopter. (b) The gripper contacts the handle of an object (260 g) and closes. (c) The gripper keeps the holding state and lifts up the object when the quadcopter flies up. (d) Once the quadcopter lands on the ground, the force applied on the extended fingers is removed, the extended fingers will open to release the object. (e) The gripper can grasp a container with a handle (225 g) without landing on the ground.

case, the drone may not be able to grasp a lightweight object (i.e., it might be impossible to find a valid range for  $k_b$  given the object’s weight). To solve this problem, we can exploit the upward acceleration of the drone to ensure a sufficient  $F_u$  for a successful state transition. Third, also for grasping, the height of objects should be large enough to allow the gripper to enclose the rod on the object. Finally, since no actuator is used for the gripper, we need to ensure there will be an object enclosed inside the extended finger from  $S_o$  to  $S_c$ . Otherwise, the gripper will need to be manually reset to  $S_o$ .

## VI. CONCLUSION

In this work, we designed, analyzed, and characterized a mechanically intelligent and passive (MIP) gripper for aerial perching and grasping. Initially open, the gripper can close by utilizing the impact force between the gripper and an object, hold the closed configuration by external weights, and automatically open when weights are removed. We established

models that can accurately predict the required force to open or close the gripper. Based on the models, we also establish design guidelines for the gripper to ensure successful perching/grasping. Various experiments are conducted to demonstrate aerial perching and grasping by placing the gripper onto a quadcopter. Since the gripper is lightweight compared with the quadcopter (up to 0.75%), we expect the MIP gripper to be ideal for aerial perching to enable long-duration monitoring tasks and aerial grasping to carry heavy payloads.

## REFERENCES

- [1] W. R. Roderick, M. R. Cutkosky, and D. Lentink, “Touchdown to take-off: at the interface of flight and surface locomotion,” *Interface focus*, vol. 7, no. 1, p. 20160094, 2017.
- [2] P. Liu, S. P. Sane, J.-M. Mongeau, J. Zhao, and B. Cheng, “Flies land upside down on a ceiling using rapid visually mediated rotational maneuvers,” *Science advances*, vol. 5, no. 10, p. eaax1877, 2019.
- [3] K. Hang, X. Lyu, H. Song, J. A. Stork, A. M. Dollar, D. Krasic, and F. Zhang, “Perching and resting—a paradigm for uav maneuvering

- with modularized landing gears," *Science Robotics*, vol. 4, no. 28, p. eaau6637, 2019.
- [4] J. Thomas, M. Pope, G. Loianno, E. W. Hawkes, M. A. Estrada, H. Jiang, M. R. Cutkosky, and V. Kumar, "Aggressive flight with quadrotors for perching on inclined surfaces," *Journal of Mechanisms and Robotics*, vol. 8, no. 5, 2016.
- [5] H. Zhang, B. Cheng, and J. Zhao, "Optimal trajectory generation for time-to-contact based aerial robotic perching," *Bioinspiration & Biomimetics*, vol. 14, no. 1, p. 016008, 2018.
- [6] M. Sitti, "Physical intelligence as a new paradigm," *Extreme Mechanics Letters*, vol. 46, p. 101340, 2021.
- [7] M. Kovac, "Learning from nature how to land aerial robots," *Science*, vol. 352, no. 6288, pp. 895–896, 2016.
- [8] H. Zhang, E. Lerner, B. Cheng, and J. Zhao, "Compliant bistable grippers enable passive perching for micro aerial vehicles," *IEEE/ASME Transactions on Mechatronics*, vol. 26, no. 5, pp. 2316–2326, 2021.
- [9] D. Howard, A. E. Eiben, D. F. Kennedy, J.-B. Mouret, P. Valencia, and D. Winkler, "Evolving embodied intelligence from materials to machines," *Nature Machine Intelligence*, vol. 1, no. 1, pp. 12–19, 2019.
- [10] M. T. Pope, C. W. Kimes, H. Jiang, E. W. Hawkes, M. A. Estrada, C. F. Kerst, W. R. Roderick, A. K. Han, D. L. Christensen, and M. R. Cutkosky, "A multimodal robot for perching and climbing on vertical outdoor surfaces," *IEEE Transactions on Robotics*, vol. 33, no. 1, pp. 38–48, 2016.
- [11] W. Chi, K. Low, K. H. Hoon, and J. Tang, "An optimized perching mechanism for autonomous perching with a quadrotor," in *2014 IEEE international conference on robotics and automation (ICRA)*. IEEE, 2014, pp. 3109–3115.
- [12] K. M. Popek, M. S. Johannes, K. C. Wolfe, R. A. Hegeman, J. M. Hatch, J. L. Moore, K. D. Katyal, B. Y. Yeh, and R. J. Bamberger, "Autonomous grasping robotic aerial system for perching (agrasp)," in *IEEE/RSJ International Conference on Intelligent Robots and Systems (IROS)*. IEEE, 2018, pp. 1–9.
- [13] U. A. Fiaz, M. Abdelkader, and J. S. Shamma, "An intelligent gripper design for autonomous aerial transport with passive magnetic grasping and dual-impulsive release," in *2018 IEEE/ASME International Conference on Advanced Intelligent Mechatronics (AIM)*. IEEE, 2018, pp. 1027–1032.
- [14] P. M. Nadan, T. M. Anthony, D. M. Michael, J. B. Pflueger, M. S. Sethi, K. N. Shimazu, M. Tieu, and C. L. Lee, "A bird-inspired perching landing gear system," *Journal of Mechanisms and Robotics*, vol. 11, no. 6, 2019.
- [15] A. McLaren, Z. Fitzgerald, G. Gao, and M. Liarokapis, "A passive closing, tendon driven, adaptive robot hand for ultra-fast, aerial grasping and perching," in *2019 IEEE/RSJ International Conference on Intelligent Robots and Systems (IROS)*. IEEE, 2019, pp. 5602–5607.
- [16] C. C. Kessens, J. Thomas, J. P. Desai, and V. Kumar, "Versatile aerial grasping using self-sealing suction," in *2016 IEEE international conference on robotics and automation (ICRA)*. IEEE, 2016, pp. 3249–3254.
- [17] C. E. Doyle, J. J. Bird, T. A. Isom, J. C. Kallman, D. F. Bareiss, D. J. Dunlop, R. J. King, J. J. Abbott, and M. A. Minor, "An avian-inspired passive mechanism for quadrotor perching," *IEEE/ASME Transactions on Mechatronics*, vol. 18, no. 2, pp. 506–517, 2012.
- [18] M. L. Burroughs, K. Beauwen Freckleton, J. J. Abbott, and M. A. Minor, "A sarrus-based passive mechanism for rotorcraft perching," *Journal of Mechanisms and Robotics*, vol. 8, no. 1, 2016.
- [19] D. J. Dunlop and M. A. Minor, "Modeling and simulation of perching with a quadrotor aerial robot with passive bio-inspired legs and feet," *ASME Letters in Dynamic Systems and Control*, vol. 1, no. 2, 2021.
- [20] H.-N. Nguyen, R. Siddall, B. Stephens, A. Navarro-Rubio, and M. Kovač, "A passively adaptive microspine grapple for robust, controllable perching," in *2019 2nd IEEE International Conference on Soft Robotics (RoboSoft)*. IEEE, 2019, pp. 80–87.
- [21] W. Stewart, L. Guarino, Y. Piskarev, and D. Floreano, "Passive perching with energy storage for winged aerial robots," *Advanced Intelligent Systems*, p. 2100150, 2021.
- [22] J. Fishman, S. Ubellacker, N. Hughes, and L. Carlone, "Dynamic grasping with a "soft" drone: From theory to practice," *arXiv preprint arXiv:2103.06465*, 2021.
- [23] H. Zhang, J. Sun, and J. Zhao, "Compliant bistable gripper for aerial perching and grasping," in *2019 International Conference on Robotics and Automation (ICRA)*. IEEE, 2019, pp. 1248–1253.
- [24] L. Cao, A. T. Dolovich, A. L. Schwab, J. L. Herder, and W. Zhang, "Toward a unified design approach for both compliant mechanisms and rigid-body mechanisms: Module optimization," *Journal of Mechanical Design*, vol. 137, no. 12, p. 122301, 2015.
- [25] F. Ruggiero, V. Lippiello, and A. Ollero, "Aerial manipulation: A literature review," *IEEE Robotics and Automation Letters*, vol. 3, no. 3, pp. 1957–1964, 2018.
- [26] R. Jitosh, K. Choi, A. Foris, and A. Mazumdar, "Exploiting bistability for high force density reflexive gripping," in *2019 International Conference on Robotics and Automation (ICRA)*. IEEE, 2019, pp. 1241–1247.

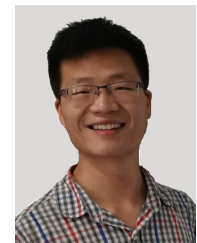
**Hao-Tse Hsiao** received his B.S. degree in Physics in 2012, M.S. degree in Opto-Electronic Engineering in 2014 from National Dong Hwa University, Taiwan. He is currently a M.S. student of Computer Engineering at Colorado State University.

His current research interests include bistable grippers and flying robots.



**Jiefeng Sun** (S'19) received his B.S. in Mechanical Engineering in 2014 from Lanzhou University of Technology, and his M.S. degree in Mechanical Engineering in 2017 from Dalian University of Technology, China. He is currently a Ph.D. student of Mechanical Engineering at Colorado State University.

His current research interests include artificial muscle, soft robots and reconfigurable robots.



**Haijie Zhang** received the B.S. degree from the School of Automation, Harbin Engineering University, Harbin, P.R. China, in 2014, and his Ph.D. degree in Mechanical Engineering from Colorado State University, Fort Collins, CO, USA, in 2021.

He currently works at Change Healthcare as a data scientist. His research interests include vision based control and flying robots.



**Jianguo Zhao** received the B.E. degree in Mechanical Engineering from Harbin Institute of Technology, Harbin, China and M.E. degree in Mechatronic Engineering from Shenzhen Graduate School, Harbin Institute of Technology, Shenzhen, China, in 2005 and 2007, respectively. He received his Ph.D. degree in Electrical Engineering from Michigan State University, East Lansing, Michigan, USA, in 2015.

He is currently an Associate Professor at Colorado State University and the director of Adaptive Robotics Lab. His research interests include soft robots, flying robots, and reconfigurable robots. He currently serves as a technical editor for IEEE/ASME Transactions on Mechatronics.